2

Conf-920124--30

UCRL-JC-109470
PREPRINT

Microchannel Heatsinks for High Average Power Laser Diode Arrays

R. Beach, B. Benett, B. Freitas, D. Ciarlo, V. Sperry,
B. Comaskey, M. Emanuel, R. Solarz, D. Mundinger

This paper was prepared for submittal to the
SPIE 1992
Los Angeles, CA
January 19-25, 1992

January 1992

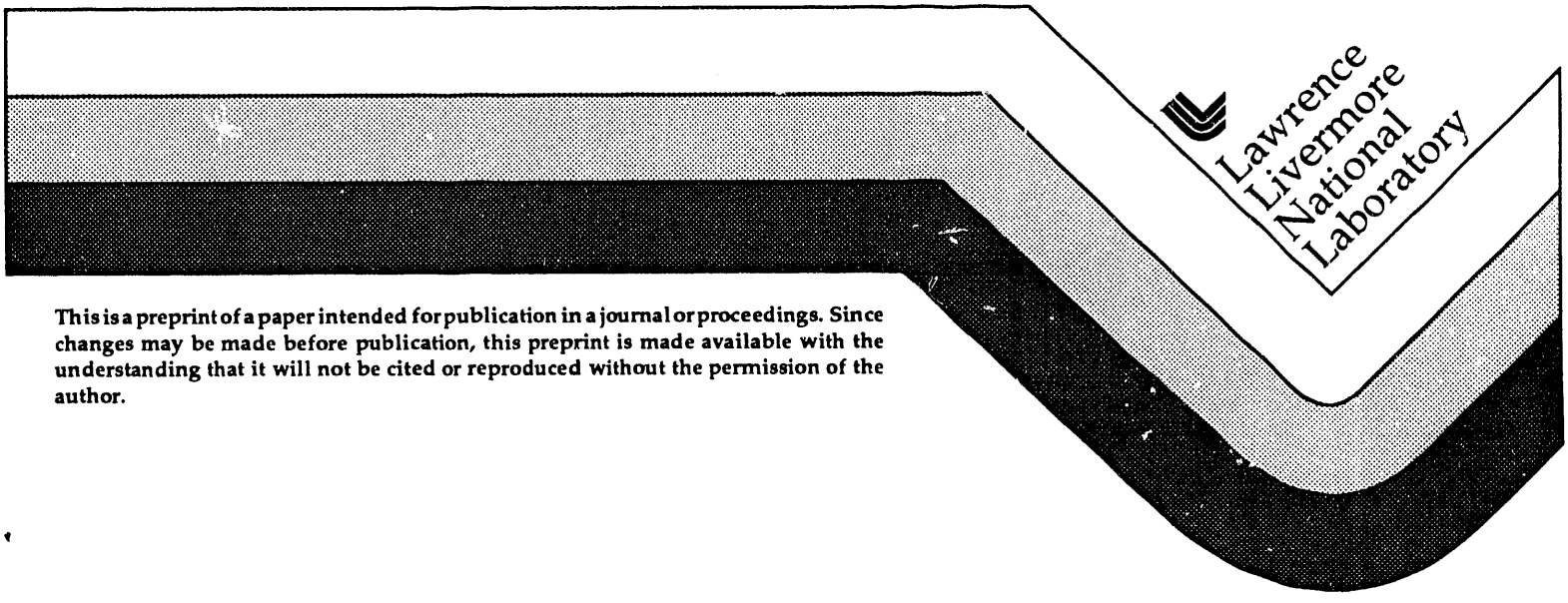

DISCLAIMER

Microchannel Heatsinks for High Average Power Laser Diode Arrays

R. Beach, B. Benett, B. Freitas, D. Ciarlo, V. Sperry
B. Comaskey, M. Emanuel, R. Solarz, and D. Mundinger
Lawrence Livermore National Laboratory
P.O. Box 808, L-495
Livermore, California 94550
(415) 423-8986

Abstract

Detailed performance results and fabrication techniques for an efficient and low thermal impedance laser diode array heatsink are presented. High duty factor or even CW operation of fully filled laser diode arrays is enabled at high average power. Low thermal impedance is achieved using a liquid coolant and laminar flow through microchannels. The microchannels are fabricated in silicon using a photolithographic pattern definition procedure followed by anisotropic chemical etching. A modular rack-and-stack architecture is adopted for the heatsink design allowing arbitrarily large two-dimensional arrays to be fabricated and easily maintained. The excellent thermal control of the microchannel cooled heatsinks is ideally suited to pump array requirements for high average power crystalline lasers because of the stringent temperature demands that result from coupling the diode light to several nanometers wide absorption features characteristic of lasing ions in crystals.

Introduction

Semiconductor lasers are inherently efficient devices capable of generating very high peak powers. Because of their compact size, the peak heat flux generated by these devices at the interface where the diode material is soldered to the chip carrier is on the order of 1 kW/cm^2, even at electrical-to-optical conversion efficiencies of 50-60% (typical of the best efficiencies reported worldwide). This thermal load, combined with the necessity to operate the devices near room temperature, is the limiting factor in the average power operation of currently available laser diodes. In an effort to facilitate high average power operation of these devices, various

packaging architectures that include integral active heatsinks have been developed. The approaches used can be broadly categorized in two groups: those that use backplane cooling, in which many laser diode arrays are mounted on one heatsinking structure, and those that use an individual heatsink for each diode bar.

The primary mission for this heatsink package is the construction of large two-dimensional diode laser pump arrays for exciting crystalline solid state lasers. The modular approach allows easy maintenance of these pump arrays; and because no tests are performed on the diode bars prior to soldering them to their heatsinks, the ability to easily interchange small sections of larger arrays is critical. The modular package approach also allows easy characterizations to be performed, enabling similarly performing diode packages to be grouped together in larger arrays. This, for example, allows good wavelength uniformity to be achieved in large arrays using an appropriate selection criterion.

Figure 1 depicts a prototype package in which an individual diode bar is attached to its own heatsink which in this case is a microchannel-based design in silicon.[1] The modular approach used here offers the potential of large and easily maintained two-dimensional apertures by simply stacking individual modules. Thermal performance was optimized by mounting the bar junction side down directly to the heatsink. The microchannel cooling technology used, originally developed for cooling wafer scale integrated circuits,[2,3] resulted in an unsurpassed thermal impedance of 0.014°C-cm^2/W. Device reliability was excellent with extrapolated current doubling lifetimes of more than 10^{11} shots. The choice of microchannel technology for the heatsink over competing impingement (turbulent flow) technology was based on several considerations: (1) the microchannel technology offers lower thermal impedances than are possible with presently available impingement coolers; (2) the fabrication of the microchannel structures relies on a previously well-developed anisotropic silicon etching technology,[4] resulting in a simple fabrication procedure; and (3) laminar flow devices such as microchannel coolers are inherently more efficient than turbulent flow devices in terms of the hydraulic power that must be expended to achieve the thermal impedances required for the diode cooling application.[3]

Present Package Design and Fabrication

The demonstrated reliability, low measured thermal impedance, easy maintainability, and simple fabrication of the prototype module depicted in Fig. 1 has led to the development of the present modular package, a photograph of which is shown in Fig. 2a. Using silver filled (conductive) silicone elastomer gaskets patterned with the same through-holes as the cooler module as shown in Fig. 2b, arbitrarily large two-dimensional apertures can be assembled by simply stacking modules. The modules of the resulting stack are thus connected electrically in series. Figure 3 shows two examples of such two-dimensional arrays fabricated by stacking 16 modules in one case and 41 modules in the other.

The module shown in Fig. 2 consists of three layers in a silicon-glass-silicon sandwich configuration. Figure 4a shows these three components. The top microchannel layer of silicon is used to supply water from the inlet port to the etched microchannels just below the location of the laser diode. The central glass insert is slotted and has through-holes matching the silicon layers. These features are fabricated using an ultrasonic machining technique. The purpose of the slot running parallel and close to the front of the glass piece in Fig. 4a is to allow the water that exits the microchannels to flow to the bottom piece of silicon which contains a manifold that delivers the water to the output port. Figure 4b shows the three pieces in a cross-sectional view and illustrates the flow path followed by the water. The thicknesses of the silicon-glass-silicon sandwich and silicone rubber gasket are approximately 1.55 and 0.30 mm, respectively, yielding a stacking density of 5.4 packages per centimeter.

The silicon microchannel layers and manifold layers are produced at the wafer scale using an anisotropic etching procedure. Six individual module layers are etched on a 3-inch wafer as shown in Fig. 5. The silicon wafers used are 381 microns thick, (110) oriented, and have a resistivity of greater than 300 Ω-cm. An 800 Å SiN layer is deposited on the wafers and appropriately patterned using a photolithographic process to define those areas of the wafer that are to be etched. The wafers are then etched in a 44% KOH solution at 35°C. The approximate etch rate is 4 μm/hr with the exact rate being dependent on the particular feature size being etched. A cross sectional view of the etched microchannels is shown in Fig. 6. The channels are nominally 25 μm wide on 50 μm centers, 150 μm deep and 1.4 mm

long. It is this finned structure and the laminar flow of cooling water through it that accounts for the unique cooling capability of the package. Rather than give a detailed discussion on the optimization procedure that was followed to design the microchannels, the interested reader is referred to the excellent treatment given in Ref. 3.

The three layers of the module are joined using a field assisted bonding procedure.[5] In this process the three components are placed in contact on a fixture and held in alignment with one another by pins as shown in Fig. 7. The assembly is then heated in an oven to 560°C, the annealing temperature of the borosilicate glass insert. Using the glass as a negative electrode and the two silicon layers as positive electrodes, an increasing voltage difference is applied in 100 V increments up to 500 V over a period of 45 minutes. The resulting electrostatic force pulls the glass and silicon into intimate contact, forming a very strong bond at the interface. The parts are annealed at high temperature for approximately two hours then allowed to cool and are removed from the oven. The wafer assemblies are then diced into individual heatsinks by a programmable silicon dicing saw.

The patterned metallization scheme visible in Fig. 2 is applied using the fixture shown in Fig. 8. In this way 32 coolers can be metallized in a single run. The metal layers are applied by sputtering. Starting at the silicon and going out, the layers are: 1000 Å of Ti; 1000 Å of Pt; 9 μm of Au; 1000 Å of Pt; and 1000 Å of Au. The thick Au ensures a low resistance current path for the up to 250 amps of current that are run through the packages. The module is metallized on its top, bottom, and front edge, with a break in the metallization that runs just below the diode bar and around the package perimeter as is visible in Fig. 2a. This scheme electrically connects the the top metallized strip of the package on which the bar is attached to the bottom of the package and gives another isolated metal pad that covers most of the top surface of the module. A 3 micron layer of indium is then evaporated to form an indium pad above the microchannels. This indium layer is the reason the second layer of Au is applied to the cooler as a thin Au layer is necessary for a high-quality indium solder joint. The 1.8 cm laser diode bar is centered directly above the microchannels on the indium pad and soldered p-side down in an H_2 atmosphere at approximately 200°C. This length of diode array is realized by using two 9 mm long bars end to end. The final step is wire bonding from the n-side of the bar to the module n-side Au contact. This is accomplished using approximately 200 1.25-mil-diameter Au wires.

The entire bottom of the package (the side not visible in Fig. 2a) is then the p-side contact.

Thermal Performance

The most important parameter characterizing a laser diode heatsink package is its measured thermal resistance - the derivative of the temperature measured at the diode junction with respect to the thermal power dissipated at the junction. It is common practice to normalize the thermal resistance quoted in units of [°C/W] to the area of the bar, giving a parameter that we refer to as the thermal impedance and having units of [°C-cm^2/W]. The most convenient way to measure the temperature of the active junction of the diode is to monitor the wavelength of the laser emission. The measurements presented herein were performed using double quantum well GRINSCH AlGaAs laser diode bars supplied by Siemens with cavity lengths of 330 microns. These bars were composed of isolated groups of 12 evanescently coupled emitters on 143 μm centers. By mounting a laser bar on a copper heatsink whose temperature could be varied and using short pulses at a low duty factor so as not to thermally load the heatsink, it was determined that $d\lambda/dT = 0.24$ nm/°C. Figure 9 shows the measured temperature rise in the diode active region against the dissipated thermal power at the junction for a 1.8 cm of diode array operating CW on one of our standard cooler modules. The dissipated thermal power was calculated by measuring the supplied electrical power to the device and subtracting the optical output power as measured by a calibrated photodiode in an integrating sphere. The data presented in Fig. 9 were acquired with a 50 psi pressure drop across the module which resulted in a 5 cm^3/s flow of water through the microchannels. This flow and pressure corresponds to an input hydraulic power of 1.74 W. Calculating the slope of the least-squares straight line fit to the data gives a measured value for the thermal resistance of 0.23 °C/W.

A simple model can accurately account for the dependence of the module thermal impedance on pressure drop across and fluid flow through the microchannels. In what follows, pressure drops are measured as pressure differences between the elongated fluid inlet and outlet ports visible in Figs. 2a and 2b. Figure 10 shows a plot of the measured water flow through a module as a function of pressure drop. The observed dependence is approximately linear. Least-

squares fitting a straight line that passes through the origin to this data gives a slope of 0.10 cm^3/s-psi. Assuming a constant thermal boundary layer in the microchannels - an excellent approximation for the flow regime of interest - gives rise to a simple two-component model for the package thermal impedance. One component results from heat flow between the thermal source in the active region and the flowing water in the microchannels. Once the thermal energy finds its way into this flowing water it is effectively swept from the module. The second component results from the caloric heating of the water as it flows through the microchannels. This second component is expected to be inversely proportional to the volume flow rate through, or equivalently the pressure drop across, the module leading to the functional form

$$R_{th} = C_1 + C_2/P \tag{1}$$

where C_1 and C_2 are as yet unknown constants and P is the pressure drop across the package. To determine the two unknown constants in Eq. 1, a standard module containing 1.8 cm of diode array was operated while monitoring the emission wavelength as a function of the pressure drop across the device. For this measurement the laser was operated at a CW optical output power of 20 W and it was determined that 73 W of thermal power was dissipated. The measured centroid emission wavelength is plotted against the inverse of the pressure drop in Fig. 11. Fitting a least-squares line to the data it is determined that $d\lambda/dP = -(26.3/P^2)$ nm-psi which can now be used to find dR_{th}/dP because

$$\begin{aligned} dR_{th}/dP &= (1/P_{th}) \bullet (d\lambda/dP)/(d\lambda/dT) \\ &= (1/73\ W) \bullet [-(26.3/P^2)\text{nm-psi}]/(.24\ \text{nm}/^\circ\text{C}) \\ &= (-1.50/P^2)\ ^\circ\text{C-psi/W}. \end{aligned} \tag{2}$$

Integrating over P gives

$$R_{th} = C_1 + (1.50/P)\ ^\circ\text{C-psi/W}. \tag{3}$$

Using the already known value for the thermal impedance at a pressure drop of 50 psi (the data from Fig. 9), C_1 can now be solved for, giving

$$R_{th} = 0.20\ °C/W + (1.50/P)\ °C\text{-}psi/W. \quad (4)$$

Normalizing to the laser diode footprint of 1.8 cm x 330 microns and rewriting Eq. 4 in terms of the hydraulic power expended to force water through the microchannels gives

$$Z_{th} = (0.012)°C\text{-}cm^2/W + (2.34 \bullet 10^{-3}/\sqrt{P_{hyd}})°C\text{-}cm^2/\sqrt{W} \quad (5)$$

where P_{hyd} is the hydraulic power supplied to the package. Figure 12 plots Z_{th} vs. P_{hyd} from Eq. 5 and illustrates the principal reason that the microchannel cooling technology was chosen for this application over competing techniques. We know of no other active heatsinking technology that offers such a compact package with low thermal impedance for such a low expenditure of input hydraulic power.

Laser Diode Performance

Figure 13 displays data acquired at low duty factor (10 Hz prf and 100 μs) from one of our modules containing 1.8 linear cm of diode array. The peak optical output of 190 W (106 W/cm) at 225 amps displayed in Fig. 13a is supply limited and typical of the performance of our modules. Figure 13b displays voltage vs. drive current data indicating a slope resistance of 7.5 mΩ which is again a typical value for a module including the two conductive silicone elastomer gaskets. The effect of the series resistance is to introduce an I^2R loss term that causes the wall plug efficiency to roll over at high currents. Figure 13c plots the measured wall plug efficiency vs drive current and indicates peak efficiency operation obtains for drive currents between 90 and 115 A. From the standpoint of optimizing the high average power operation of diodes it is then desirable to operate at high duty factor in this current range. Figure 13d plots the peak dissipated thermal power for this low duty factor characterization. From these data it is evident that to optimize module efficiency at high duty factor the heatsink must have the capability of dissipating approximately 170 W while holding the active junction at a reasonable operating temperature. Using our measured thermal resistance value of 0.23°C/W and an inlet water

temperature near 0°C, our module enables CW operation of the laser diodes at a junction temperature of 40°C and at drive currents that optimize their efficiency.

Figure 14a plots CW light output from a single module as a function of supplied current. The peak optical output is 70 W (38.9 W/cm) at 100 A of input current and is supply limited at this point. The measured CW slope efficiency is 0.91 W/A and the threshold current is 21.6 A. Figure 14b plots the thermal power dissipated in the same package as a function of the input current. The maximum thermal power dissipation at 100 A of input current is 160 W which corresponds to a thermal footprint of 2.7 KW/cm^2. Even at these heat loads, evidence of thermal roll over is only just beginning to be visible. Figure 14c plots reliability data that was acquired in a constant optical power lifetest. During this test the bar was operated CW at an output power of 40 W by continuously adjusting the drive current to compensate for device degradation. At the beginning of the lifetest the thermal power dissipated was approximately 110 W and the diode junction temperature was approximately 25°C above the inlet water temperature of 15°C. The lifetest was terminated after 580 hours when the required drive current had increased by 30%. Figure 14d displays an L-I characterization curve made 400 hours into the the lifetest. The reduced performance of the diode is entirely accounted for by a degradation in the slope efficiency from an initial value of 0.91 W/A to a final value of 0.70 W/A. Again, even at the peak heat load of 2.7 kW/cm^2, evidence of thermal roll over is only barely visible indicating no degradation in the thermal performance of the heatsink.

The spectral linewidth of the emitted radiation is of the utmost importance to the performance of diode pump arrays used to excite crystalline lasers. This is due to the nm-wide absorption lines that are typically used to couple the diode radiation to the solid state laser. The effective (time-integrated) spectral linewidth of the laser is broadened by the effects of transient heating during a current pulse, an effect commonly referred to as chirp. Depending on the particular pulse width the diode is operated at, different effects can dominate the observed linewidth. Figure 15 plots the measured centroid emission wavelength from one of our modules during a 1 millisecond pump pulse. The observed chirp results from the transient heating of the diode bar and heatsink during the pulse. These spectral snapshots were acquired in 5 μs windows at increasing delays into the pulse with the package operating at a peak optical power of 100 W. For pump pulses having roughly 100 μs durations,

such as would be typical for exciting Nd^{3+}:YAG storage lasers, the effective linewidth of the pump pulse is hardly affected by transient heating and is typically on the order of 3 nm FWHM or less. For pulse widths on the order of several hundred microseconds to a millisecond the emission wavelength of the diode bar is swept toward longer wavelengths as the bar and heatsink heat up. In this regime the transient heating can effectively double the effective emission linewidth to nearly 6 nm FWHM. For very long pulse or even CW operation, that part of the emitted light that is strongly chirped due to transient heating during the first millisecond of operation contributes only a small fraction of the total energy to the pulse and the effective linewidth once again approaches 3 nm FWHM. Figure 16 displays spectral line shapes from a module operating at a peak optical power of 100 W at four different pulse widths: 100 μs, 250 μs, 500 μs, and 1 ms. In this case the line shapes are representative of the entire time-integrated pulse and have FWHM of 3.1, 3.8, 4.8 and 5.8 nm, respectively.

Another factor impacting emission linewidth is the uniformity of the thermal impedance along the bar. This can be especially important under conditions of CW operation in which the bar is operating under aggressive thermal loading. Figure 17 shows three high resolution spectral scans taken from different locations on one of the 9 mm bars that make up half of the array on a module These scans were made with the module operating at a CW optical output power of 20 W (11.1 W/cm) by imaging a small section of the near field pattern of the bar onto a spectrometer slit. In this case the spectra were acquired from regions at either end and in the center of bar. The modulation evident in the scans is due to the different longitudinal laser modes. The overlap in wavelength of these three spectra is typical of the observed emission uniformity for our heatsink and is evidence of the excellent thermal control it affords. The linewidths of 2.5 to 3 nm FWHM are also typical of the measured emission linewidths under conditions of CW operation.

Figure 18 shows the emission spectrum measured from the 41 module stack of Fig. 3b. The displayed spectra were acquired using 100 μs pulses at various current levels. To ensure that the emission of the entire array was equally sampled, the output of the stack was directed to an integrating sphere and the spectral measurement was made on a port at 90° to the entrance. At currents of 40, 80 and 140 A the observed linewidths were 2.5, 3.1 and 3.8 nm FWHM, respectively. In this

pulse width regime the increasing linewidths are due to transient heating and are indicative of the excellent performance obtainable even in very large pump arrays.

Two-Dimensional Array Assembly

Two-dimensional arrays are made by stacking the modular heatsink packages as shown in Fig. 19. Both hydraulic and electrical connections are formed by a silver-filled (conductive) silicone elastomer gasket between adjacent packages. The gasket also provides the necessary clearance between packages for the diode bars and wire bonds. Individual packages are electrically in series and hydraulically in parallel with one another. Gasket compression is applied by a single bolt through the stack in the center of the sealing area to ensure uniform loading. The amount of compression applied to the stack is repeatably set by monitoring torque on the bolt during assembly. Manifold blocks on each end of the stack serve as electrical terminals and provide inlet and outlet hydraulic connections.

Hydraulic Reliability

Two hydraulic reliability issues are critical to the success of the modular approach: (1) silicone seal integrity, and (2) clog-free operation of the 20-micron-wide microchannel cooling manifold during extended periods of operation. Reliability tests on arrays consisting of five packages have been performed to address these issues. Using a flow test system equipped with 0.2 μm filtration, a deionizing system (>18 mΩ-cm) and a UV light to inhibit biological growth. The data from this ongoing test is presented in Fig. 20 and shows a constant-pressure flow rate reduction of less than 8% for 5,000 hours of operation. No leakage from the silicone seals has been evident.

The silicone gasket material has been observed to cold flow under compression which, if not compensated for, results in loss of seal integrity when arrays are operated below ~0°C. The gaskets stabilize after approximately five days of daily re-torquing. This problem has been successfully addressed by simply incorporating a spring washer on the compression bolt.

Conclusion

A modular, actively cooled laser diode array heatsink has been developed utilizing microchannel cooling technology. The heatsink enables high duty factor or even CW operation of fully filled linear diode arrays at high average power. The laminar flow microchannel cooling technique leads to a heatsink having the very low thermal impedance required for the laser diode cooling application as well as one that is inherently efficient in terms of the hydraulic power needed to circulate the cooling fluid. As such, the developed heatsink is well suited to diode pumped solid state laser applications having very constrained weight and volume budgets. Package manufacturability has been optimized using low cost silicon as the chip carrier material and well developed silicon etching technologies to fabricate the microchannels. The modular approach used for the heatsink allows very large two-dimensional apertures to be constructed by simply stacking the packages. In these large arrays, system maintainability is enhanced by the capability to swap out individual packages. This technology is well suited to the problem of pumping crystalline solid state lasers as the excellent thermal control afforded by the heatsink package is well matched to the stringent temperature requirements placed on diode arrays that must couple to nm-wide absorption features characteristic of lasing ions in crystals. Finally, high average power diode reliability is enhanced due to the low temperature operation that the small thermal impedance enables.

Acknowledgment

This work was performed under the auspices of the U.S. Department of Energy by Lawrence Livermore National Laboratory under contract W-7405-Eng-48. The authors would like to express their appreciation and thanks to W. Krupke, G. Albrecht, and E. V. George of LLNL for many stimulating discussions during the course of this work, and to S. Mills, L. DiMercurio, J. Hamilton, E. Utterback, T. Rodriquez, S. Stockton, and L. Nguyen also of LLNL for all their help in the design and fabrication of the heatsinks.

References:

1. R. Beach, D, Mundinger, W. Benett, V. Sperry, B. Comaskey, and R. Solarz, "High-reliability silicon microchannel submount for high average power laser diode arrays," Appl. Phys. Lett. **56**, 2065 (1990).

2. D. Tuckerman and R. Pease, "High-Performance Heatsinking for VLSI," IEEE Electron. Device Lett. **EDL-2**, 126 (1981).

3. D. Tuckerman, "Heat-transfer microstructures for integrated circuits," Ph.D. thesis, Stanford University.

4. H. Seidel, L. Csepregi, A. Heuberger, H. Baumgartel, "Anisotropic etching of crystalline silicon in alkaline solutions," J. Electrochem. Soc. **137**, 3612 (1990).

5. G. Wallis and D. Pomerantz, "Field assisted glass-metal sealing," J. Appl. Phys. **40**, 3946 (1969).

Figure Captions

1. Diagram of a prototype modular package in which a single diode bar is attached to a single silicon microchannel cooler (from Reference 1).

2. a) Photograph of our modular microchannel cooled package that accepts 1.8 cm of laser diode bar. The approximate package dimensions are 2 cm x 2 cm. The diode array is mounted approximately 1.5 mm back from the top edge of the package and emits upward in the photo at grazing incidence to the metallized silicon cooler. The central through-hole is for a bolt allowing modules to be stacked to make two-dimensional arrays. The elongated holes on either side serve as water inlet and outlet. b) Cut-away drawing of the package showing the placement of the conductive silicone rubber gasket.

3. a) Operating two-dimensional laser diode array constructed by stacking 16 modular microchannel packages. b) This 42 module stack was fabricated for pumping a Nd^{3+}:YAG high average power crystalline slab laser.

4. a) The three layers of the microchannel cooled module. The borosilicate glass insert is sandwiched between two pieces of etched silicon - the manifold layer and the microchannel layer. All features on the glass piece are through-holes. On the silicon pieces the central round feature and two elongated features are through holes while the remaining patterned features are etched to a depth of approximately 150 microns. The sides of the silicon pieces not shown in the photograph are featureless except for the through-holes. b) Cross-sectional view of the three layers showing the water flow path. Each silicon layer is approximately 381 microns thick and the central glass layer is approximately 787 microns thick.

5. Etched 3 inch silicon wafers. The manifold layer is on the left and the microchannel layer is on the right.

6. Scanning electron micrograph showing a cross-sectional view of the etched microchannels. The channels and separating walls are both approximately 25 microns wide and the channel depth is approximately 150 microns.

7. Wafer components being assembled on a fixture in preparation for the field assisted bonding procedure.

8. The carousel fixture shown in the photograph is used to apply the patterned metallization to up to 32 coolers in a single sputtering run.

9. Measured temperature rise of a 1.8 cm linear diode array operating CW on our standard cooler module as a function of the thermal power dissipated in the active region. The straight line is a least-squares fit to the data and has a slope of 0.23°C/W.

10. Measured water flow rate through our standard heatsink module as a function of pressure across the device. These data were acquired at a water inlet temperature of 15°C. The straight line is a least-squares linear fit through the origin to the measured data points and has a slope of 0.10 cm^3/s-psi.

11. Emission wavelength for a standard module producing 20 W of CW optical power and dissipating 73 W of heat as a function of inverse water pressure. The slope of the least-squares fit straight line to the data is 26.3 nm-psi.

12. Thermal impedance is plotted against expended hydraulic power from Eq. 5.

13. Low duty factor characterization data from a module using 10 Hz prf and 100 μs current pulses. a) Peak optical power out vs. peak drive current. The maximum output of 190 W (106 W/cm) is supply-limited. The least-square fit straight line indicates s slope efficiency of 0.95 W/A and a lasing threshold current of 23.7 A. b) Voltage across module (including two conductive silicone rubber gaskets for sealing) vs. drive current. The least-square fit straight line indicates a series resistance of 7.5 mΩ. c) Measured wall plug efficiency vs. drive current. The observed roll off at high drive currents results from I^2R loss. Efficiency optimizes for drive currents between 90 and 115 A. d) Peak thermal power dissipated as a function of drive current.

14. a) Optical output power vs drive current from a single module operating CW. The maximum CW optical output is 70 W and is supply limited. The measured slope efficiency is 0.91 W/A. b) Dissipated thermal power vs. drive

current. At 100 A the thermal footprint is 2.7 KW/cm^2 and the temperature of the diode junction is approximately 37°C above the coolant inlet temperature of 15 °C. c) Constant optical power lifetest results. The current was continually adjusted to maintain a 40 W CW optical output power until the required current increased by 30% after 580 hours. d) An optical power vs. drive current characterization performed approximately 400 hours into the lifetest. The data indicate that device degradation is entirely accounted for by the reduced slope efficiency. No degradation in the thermal performance of the heatsink is observed.

15. Measured pulse chirp through a 1 ms, 100 W diode pulse. The data represent emission wavelength centroids for spectral snapshots acquired in 5 μs long windows at the indicated delay into the pulse.

16. Measured linewidths from a module producing 100 W of optical output at 4 different pulsewidths: 100 μs, 250 μs, 500 μs and 1 ms. The observed linewidths are 3.1, 3.8, 4.8 and 5.8 nm, respectively. In this case the emission features are representative of the integrated pulse. Longer pulse widths result in greater emission red shift due to transient heating of the bar and heatsink.

17. High resolution spectral scans made on one of the 9 mm bars that make up half the linear array on a module. The module was operated CW at a total output of 20 W. The three scans were made from radiation collected at either end and the middle of the bar. The FWHM is 2.5 to 3 nm and the good overlap of the spectra imply a uniform thermal impedance along the length of the bar.

18. Emission spectrum measured from the 41 module stack of Fig. 3b. The displayed spectra were acquired using 100 μs long current pulses at 40 , 80 and 140 amps. The observed linewidths were 2.5, 3.1 and 3.8 nm FWHM, respectively.

19. A two-dimensional microchannel cooled diode laser array being assembled.

20. The flow rate through a five heatsink stack divided by the pressure drop across the stack plotted against elapsed time.

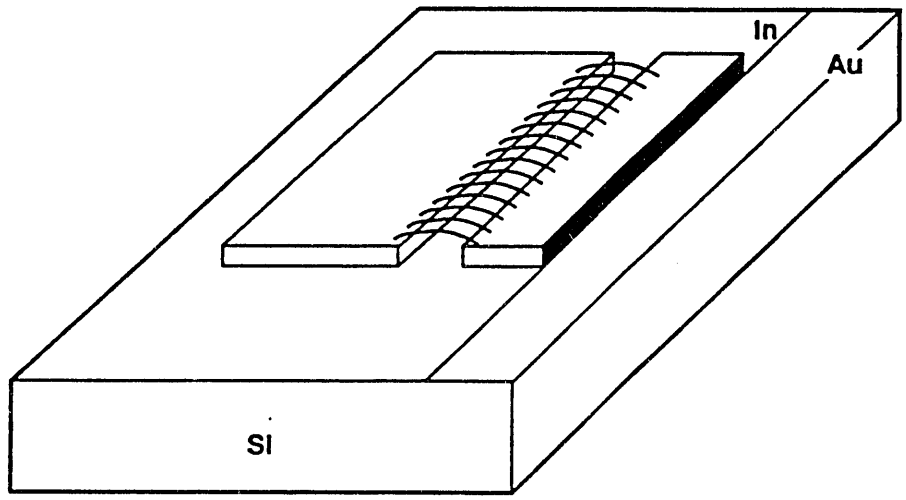

Figure 2 1

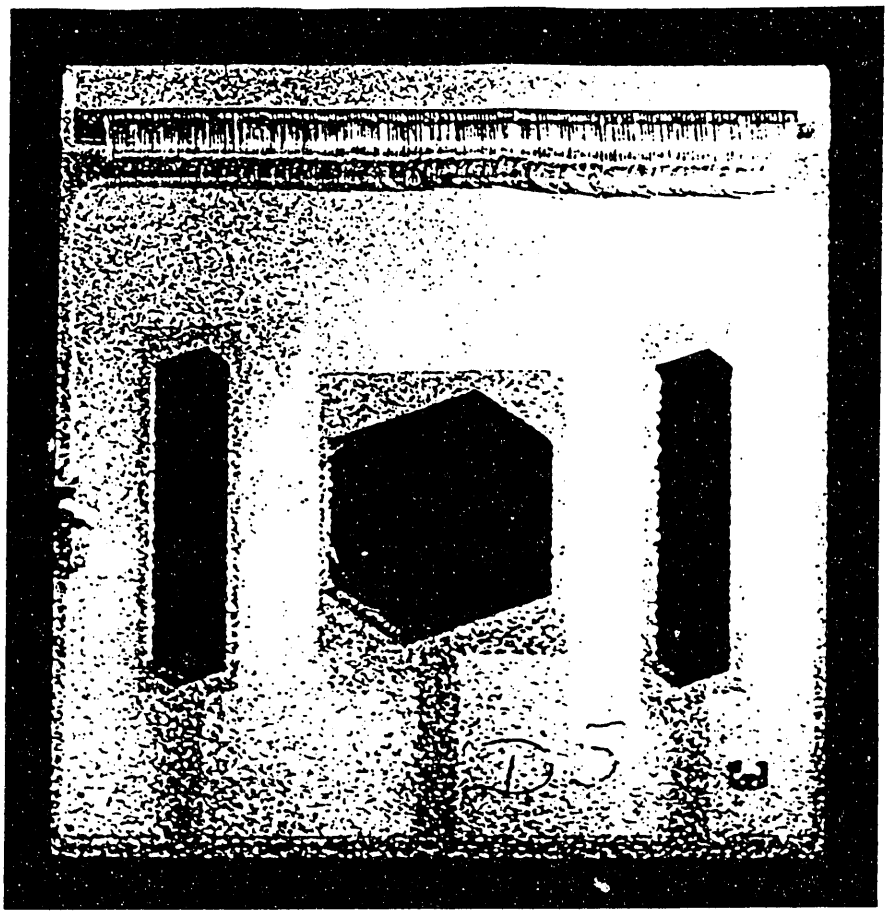

(a)

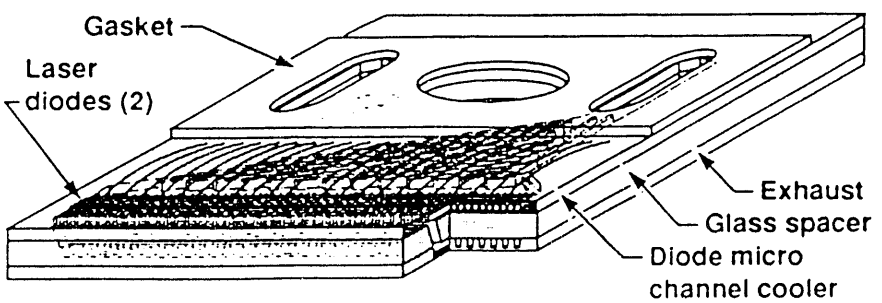
Gasket
Laser
diodes (2)
Exhaust
Glass spacer
Diode micro
channel cooler

(b)

Figure 2

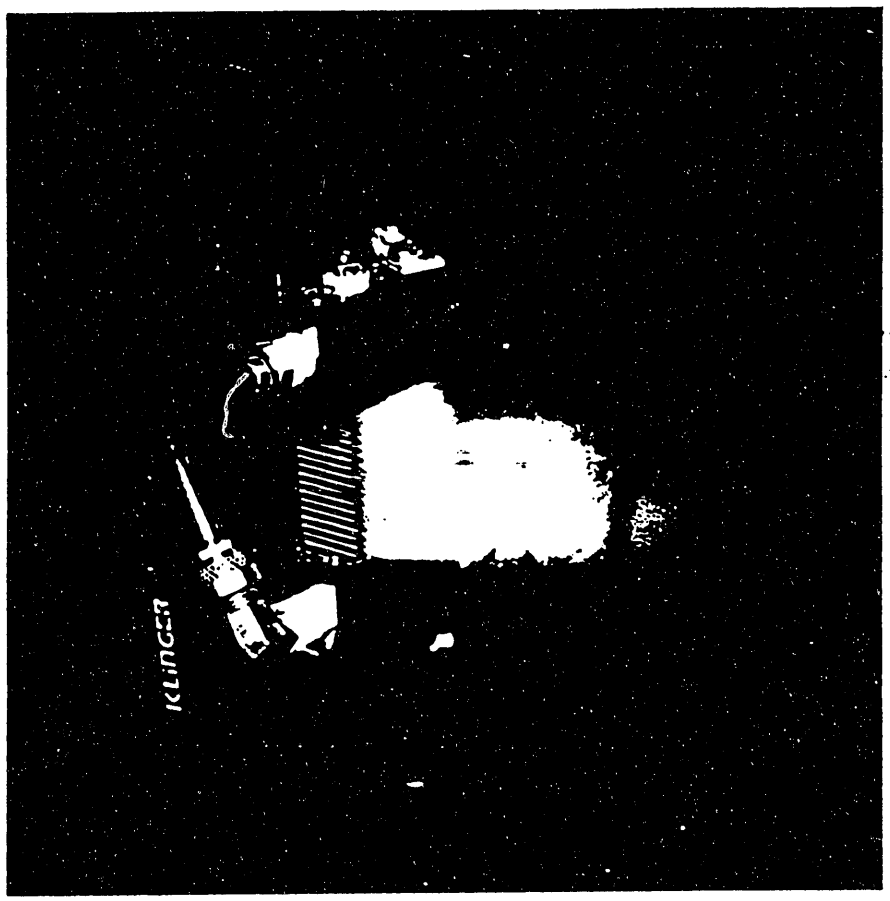

Figure ~~44~~ 39

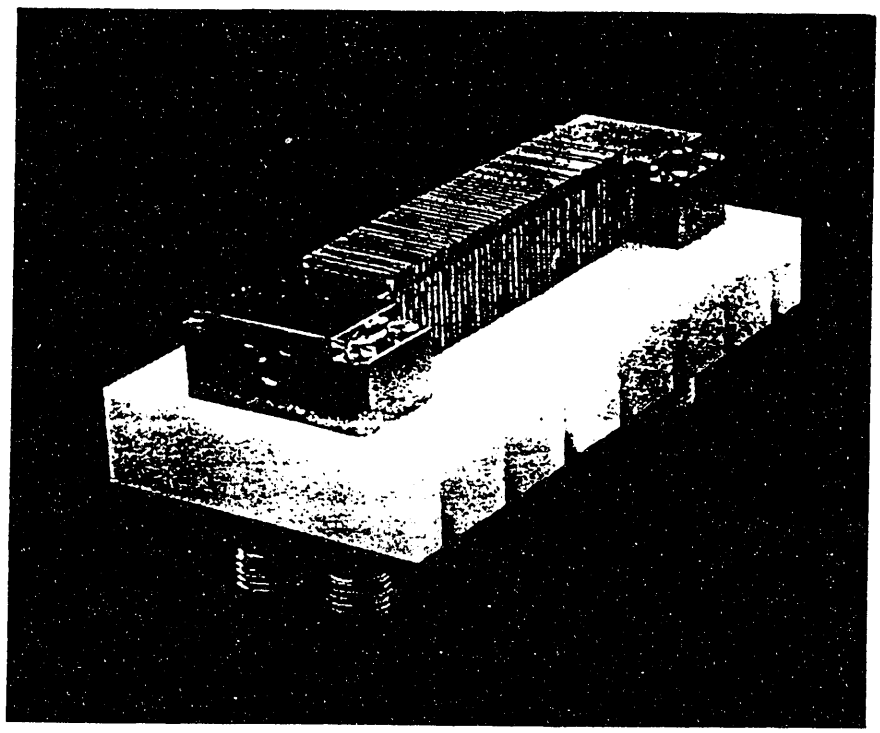

Figure ~~4b~~ 3b

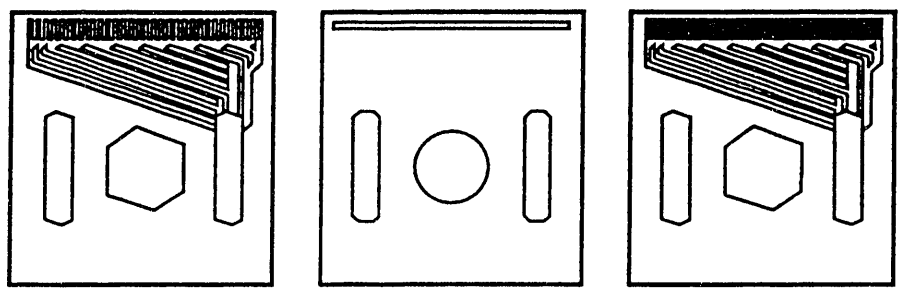

Figure ~~5a~~ 4a

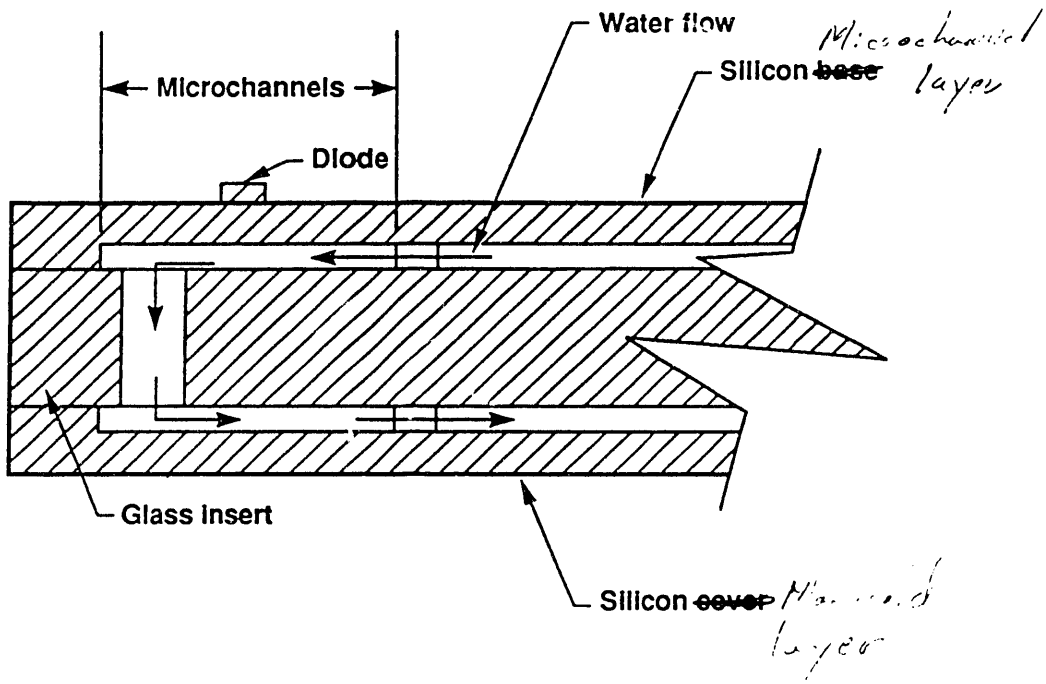
Water flow
Microchannel layer
Silicon ~~base~~
Microchannels
Diode
Glass insert
Silicon ~~cover~~ Manifold layer

Figure ~~5b~~ 4b

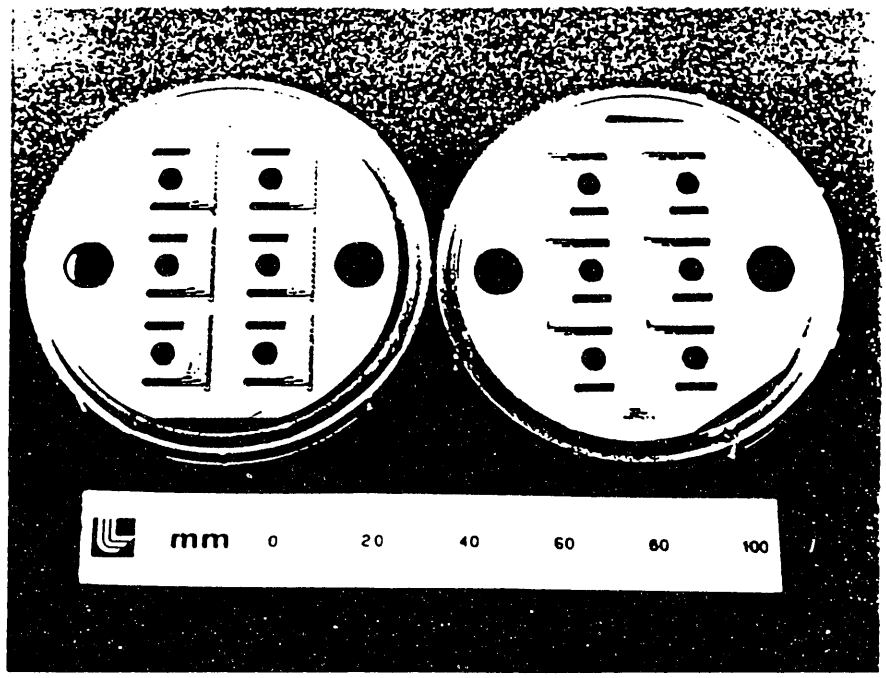

Figure 5

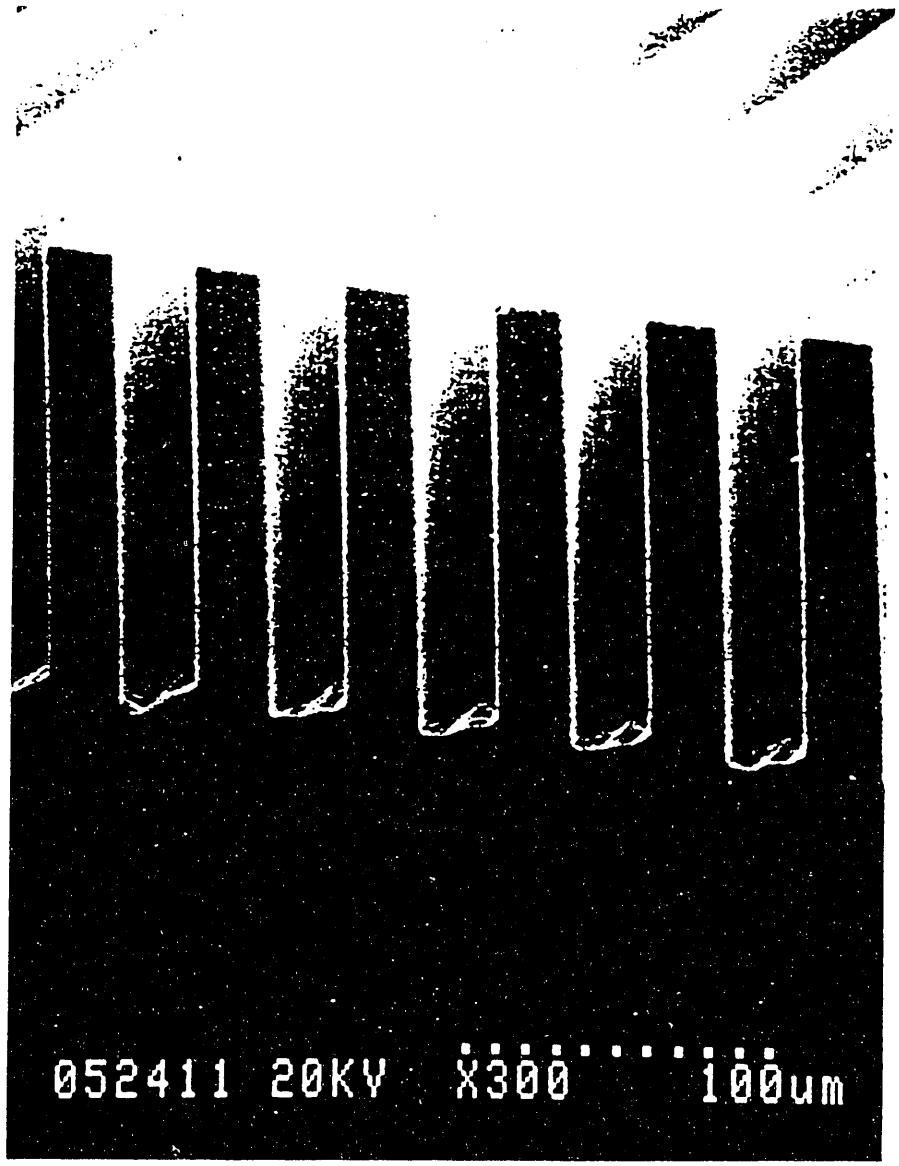

Figure 16

Fig 7

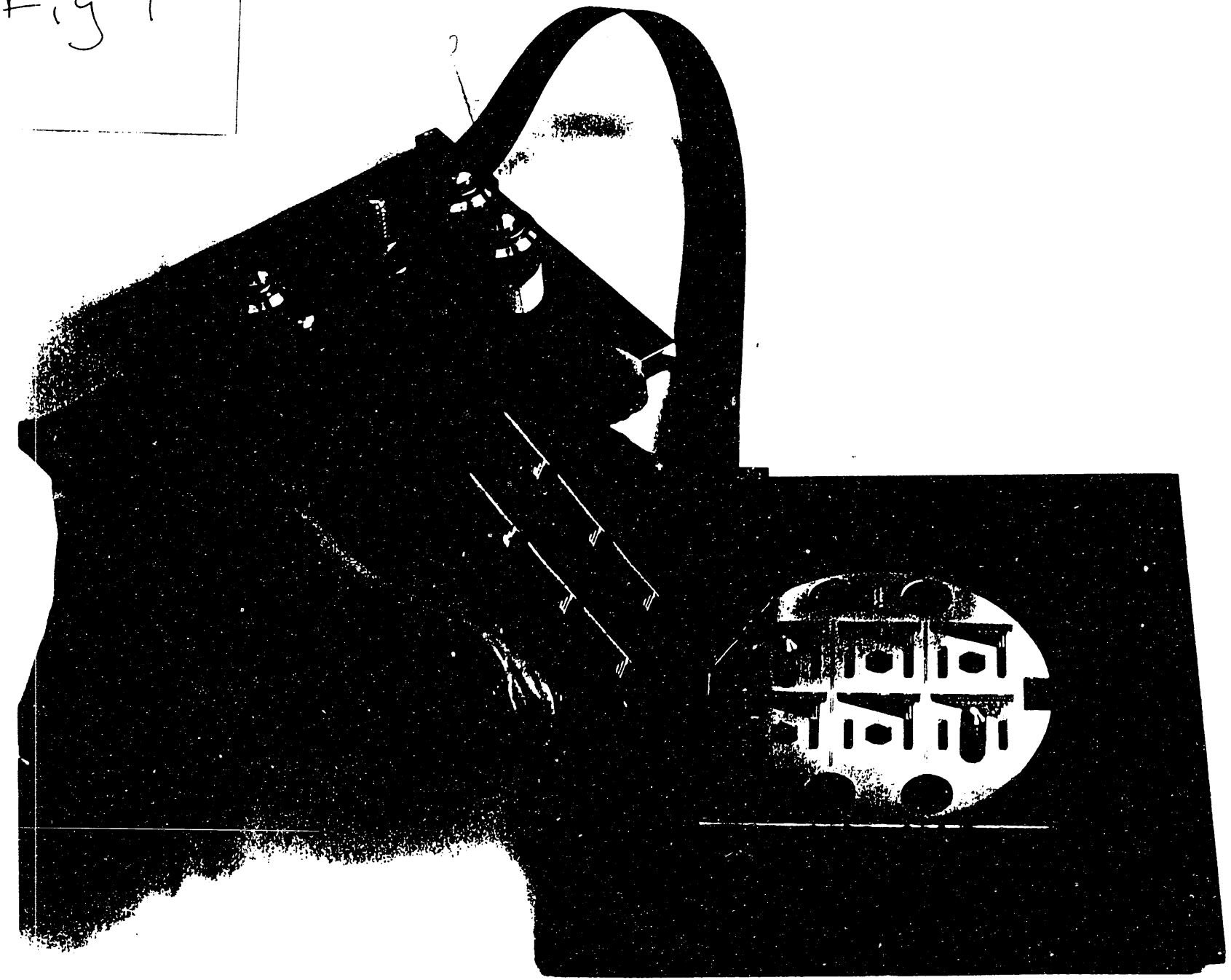

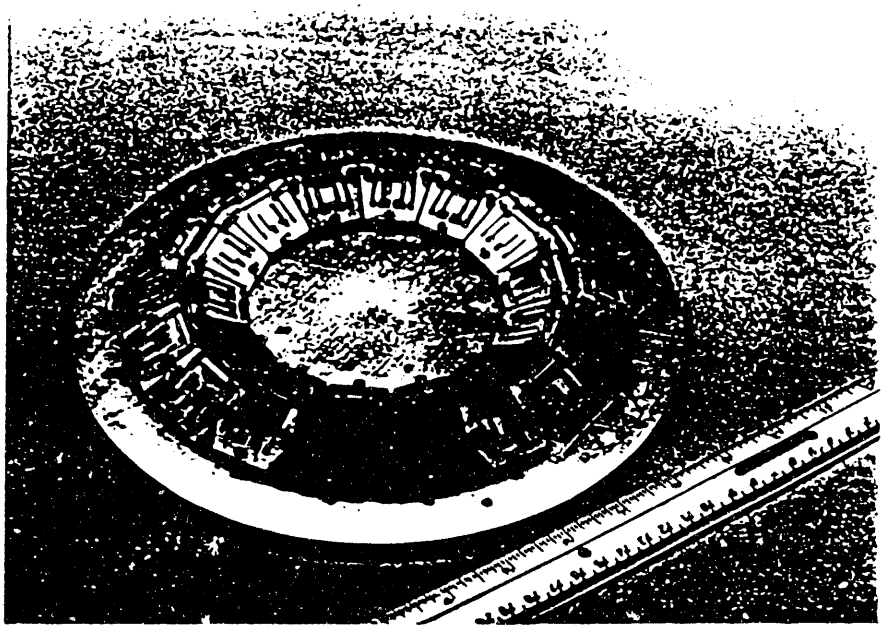

Figure 8

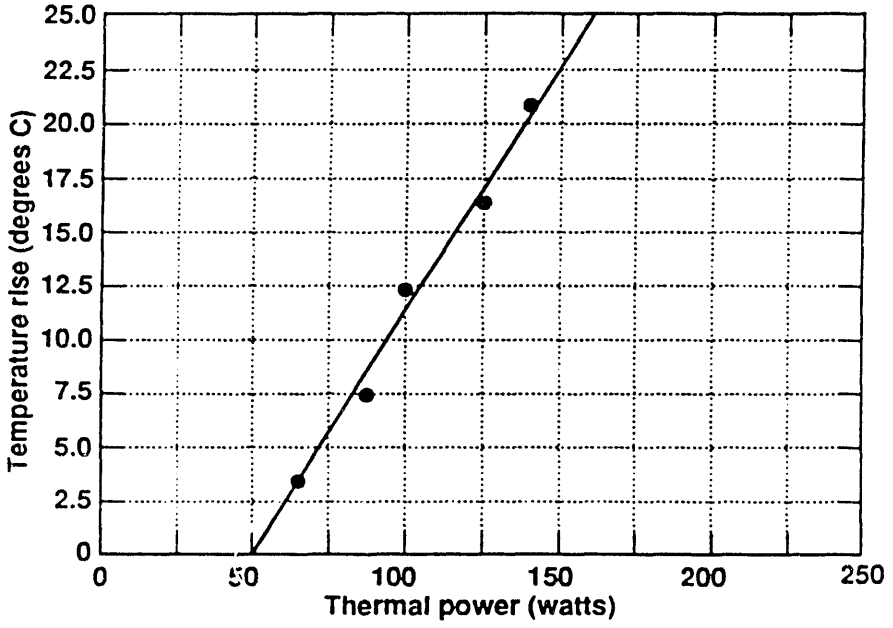
25.0
22.5
20.0
17.5
15.0
12.5
10.0
7.5
5.0
2.5
0
Temperature rise (degrees C)
0
50
100
150
200
250
Thermal power (watts)

Figure 9

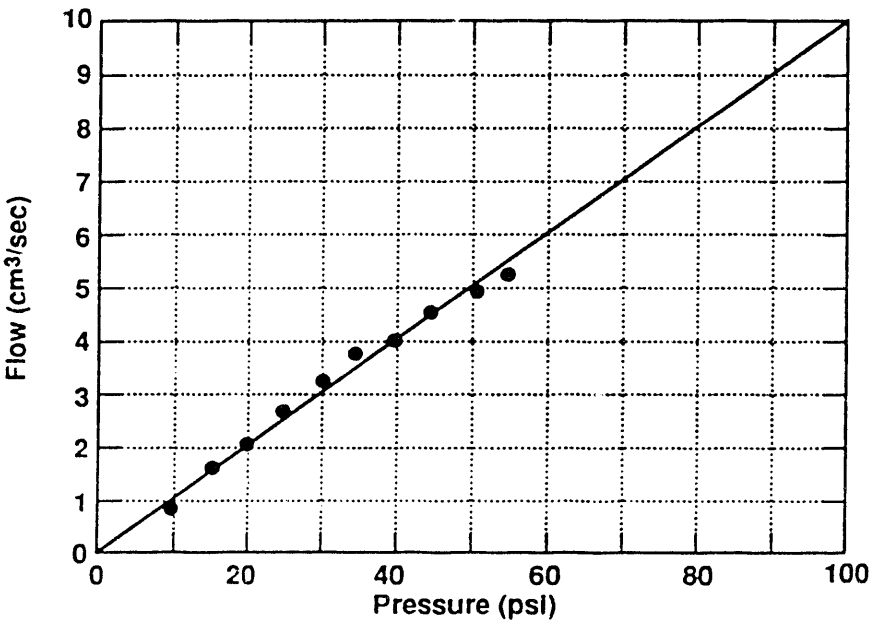

Figure 10

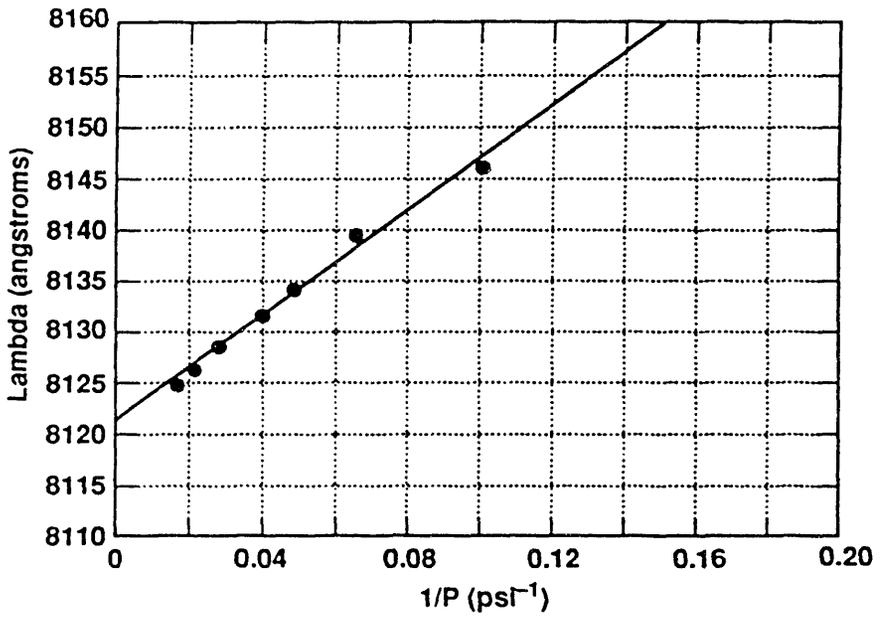

Figure 11

qt-u-j-16594-11

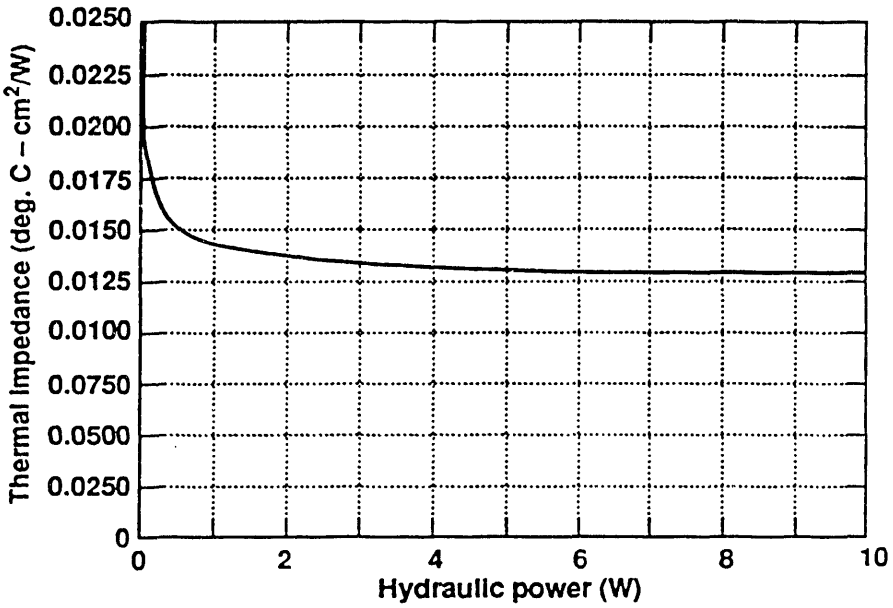
Thermal Impedance (deg. C – cm²/W)
0.0250
0.0225
0.0200
0.0175
0.0150
0.0125
0.0100
0.0750
0.0500
0.0250
0
0
2
4
6
8
10
Hydraulic power (W)

Figure 12

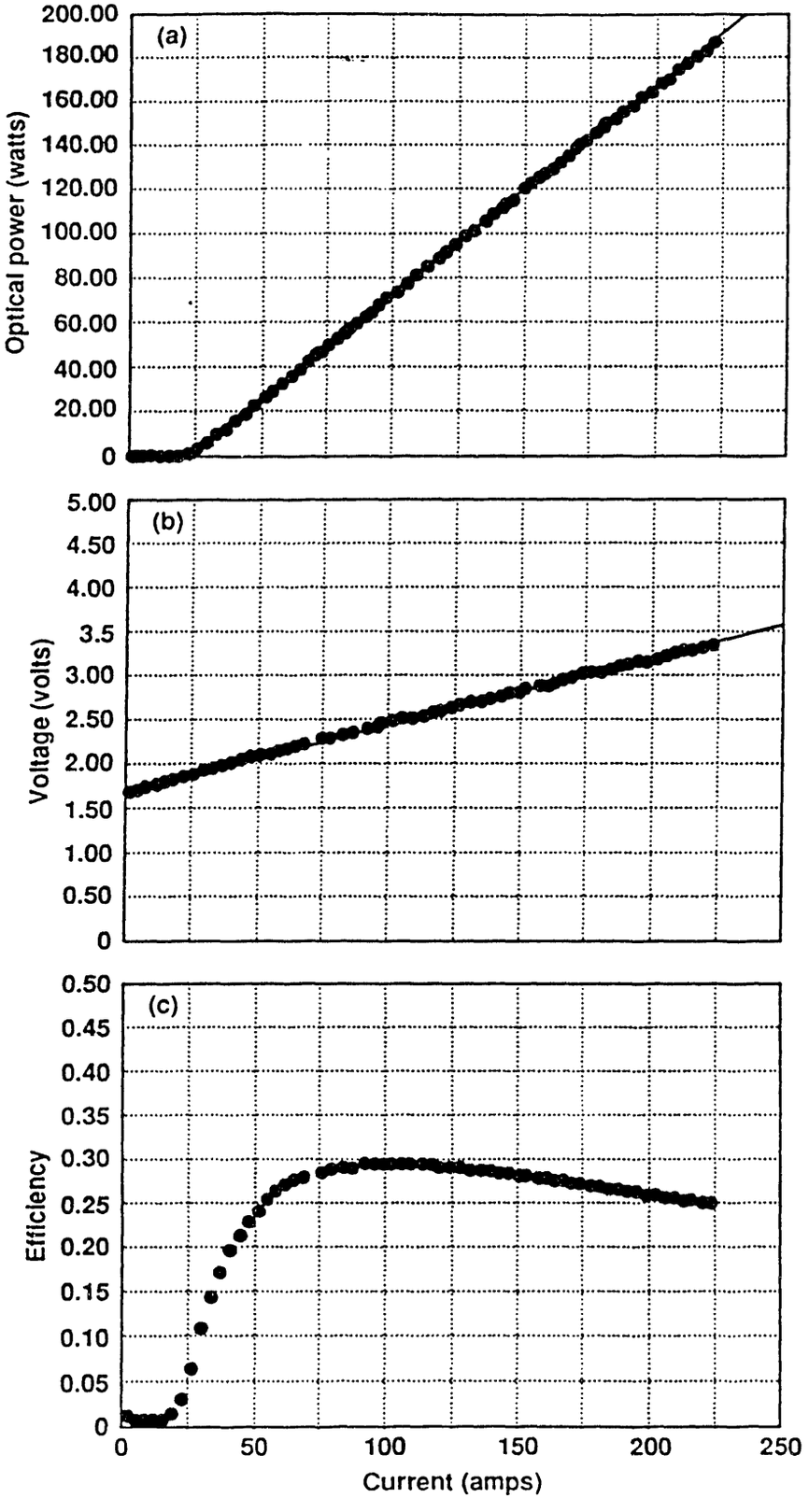

Figure 13 a b c

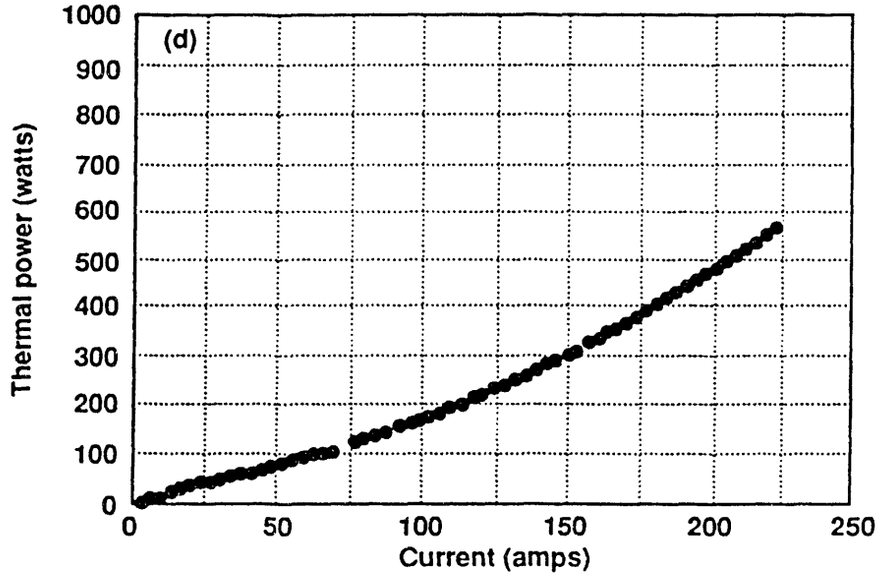
(d)
Thermal power (watts)
1000
900
800
700
600
500
400
300
200
100
0
0
50
100
150
200
250
Current (amps)

Figure 13d

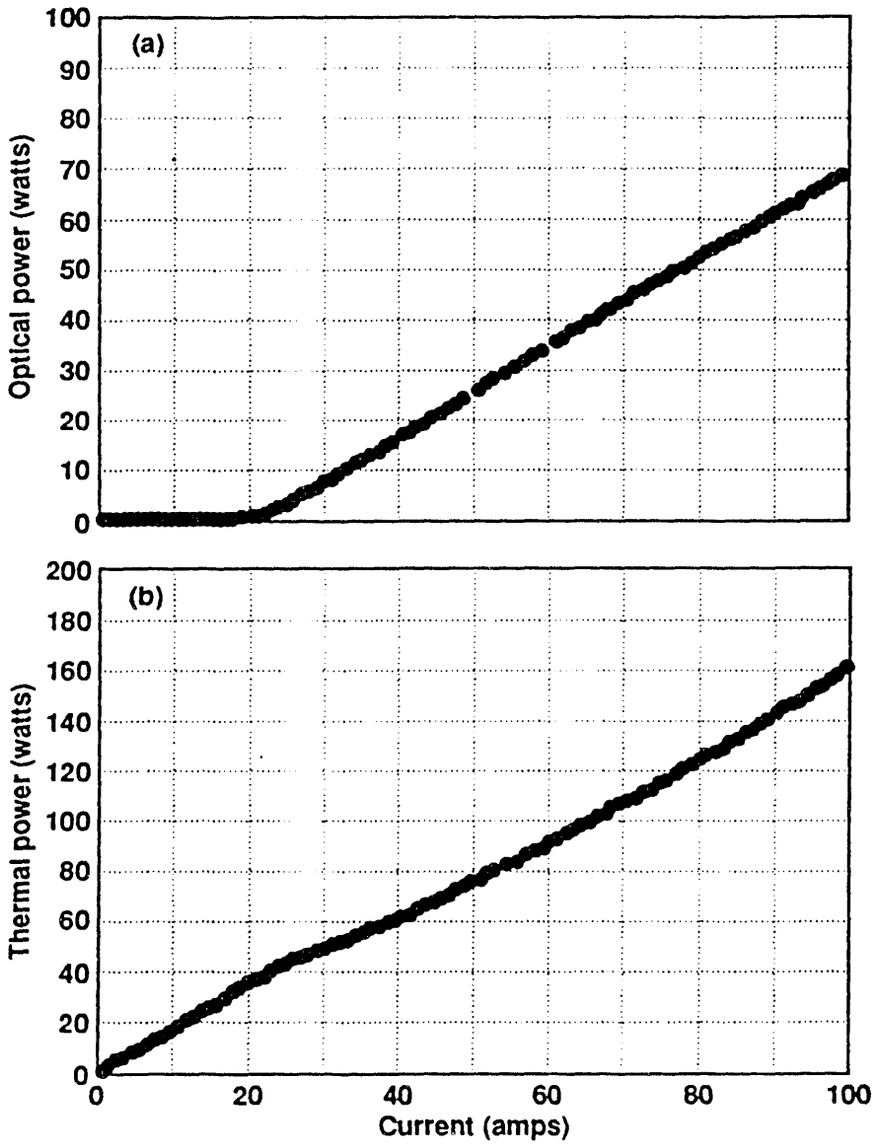
(a)
Optical power (watts)
100
90
80
70
60
50
40
30
20
10
0
(b)
Thermal power (watts)
200
180
160
140
120
100
80
60
40
20
0
0
20
40
60
80
100
Current (amps)

Figure 14 a b

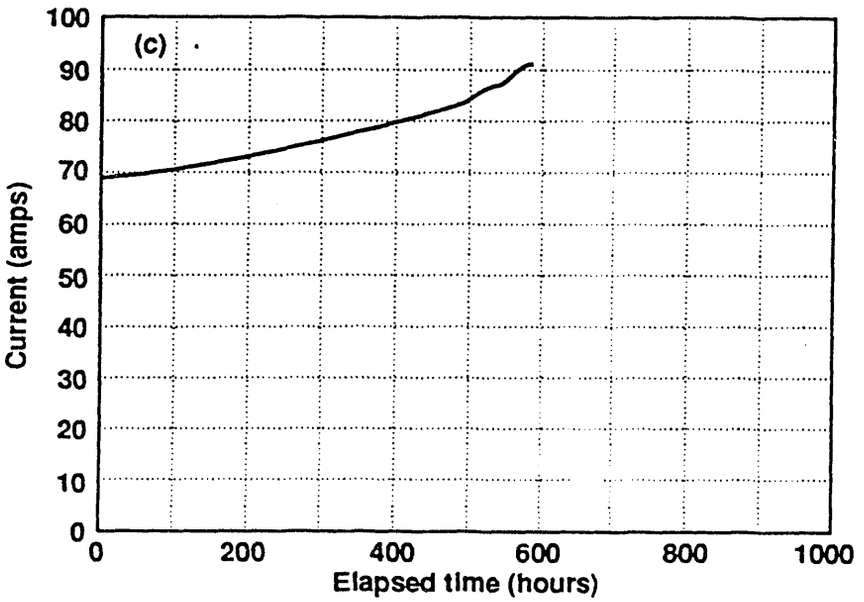
(c)
Current (amps)
100
90
80
70
60
50
40
30
20
10
0
0
200
400
600
800
1000
Elapsed time (hours)

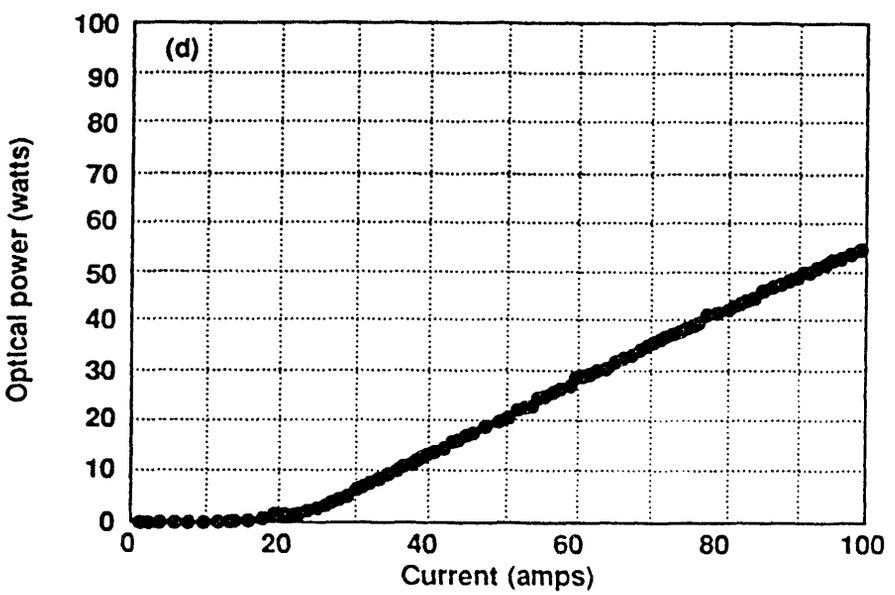
(d)
Optical power (watts)
100
90
80
70
60
50
40
30
20
10
0
0
20
40
60
80
100
Current (amps)

Figure 14 c d

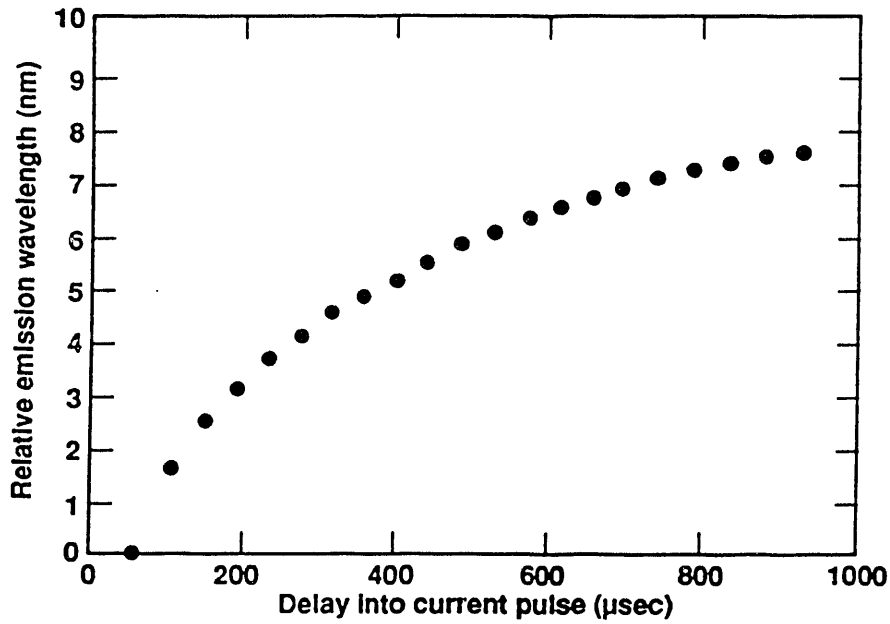
Relative emission wavelength (nm)
0
1
2
3
4
5
6
7
8
9
10
0
200
400
600
800
1000
Delay into current pulse (μsec)

Figure 15

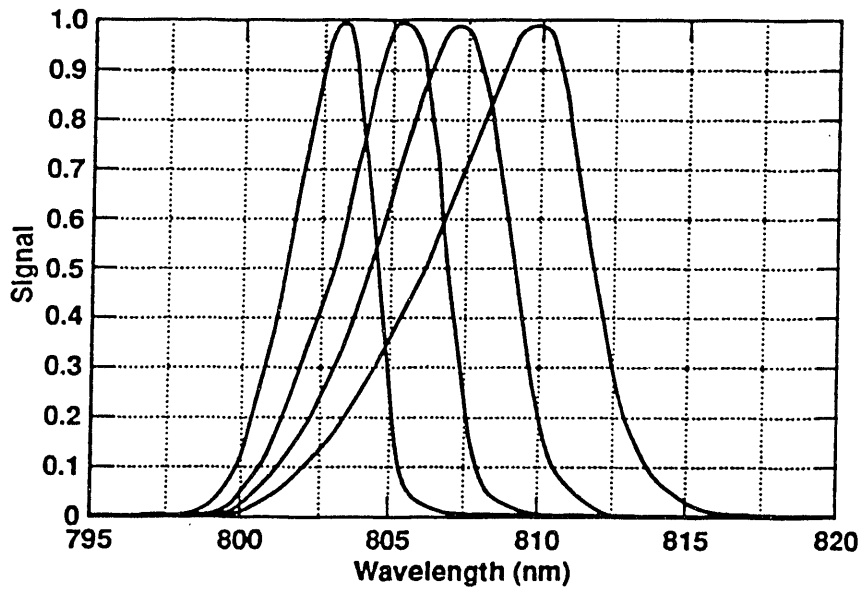
1.0
0.9
0.8
0.7
0.6
0.5
0.4
0.3
0.2
0.1
0
Signal
795
800
805
810
815
820
Wavelength (nm)

Figure 16

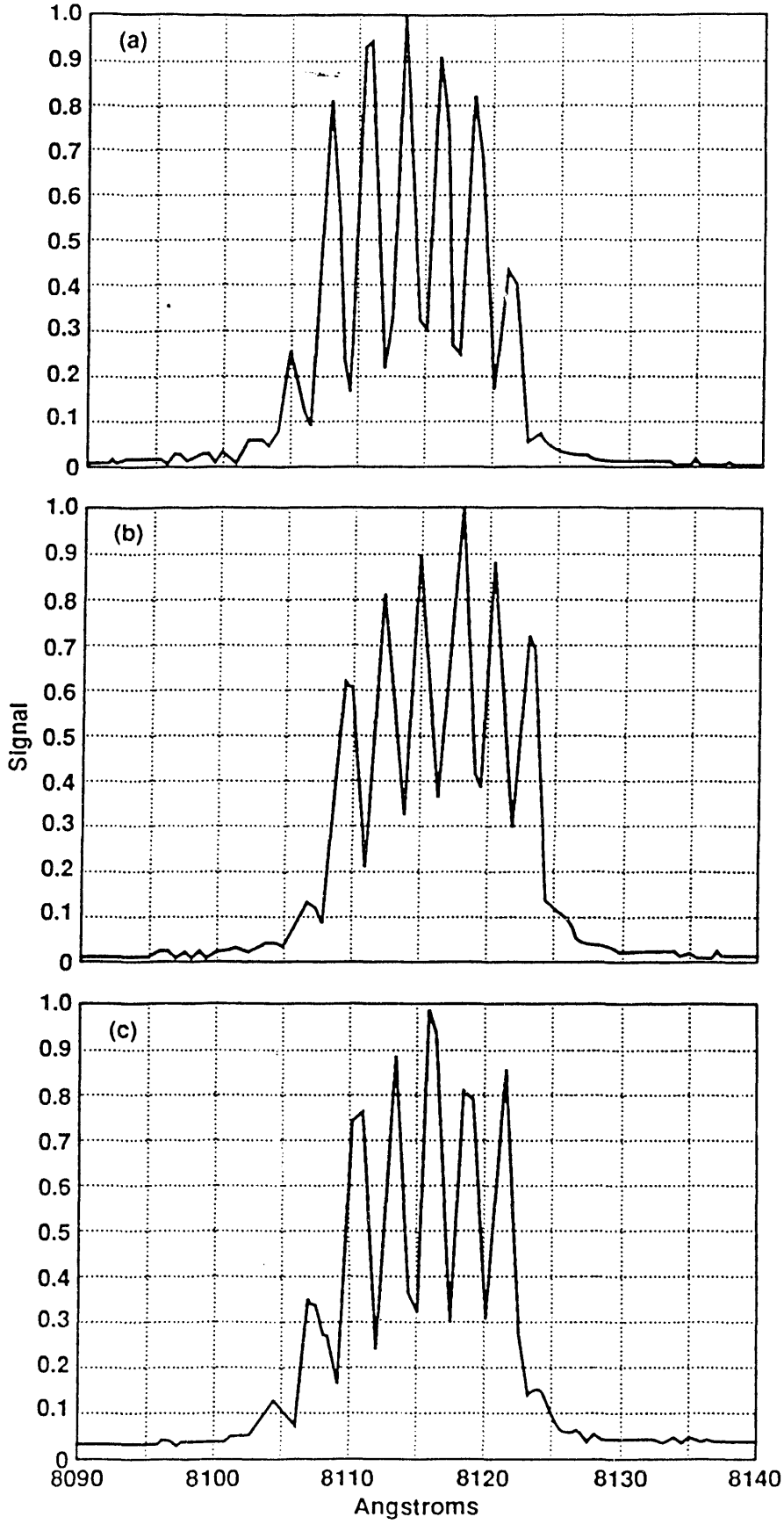

Figure 17 a b c

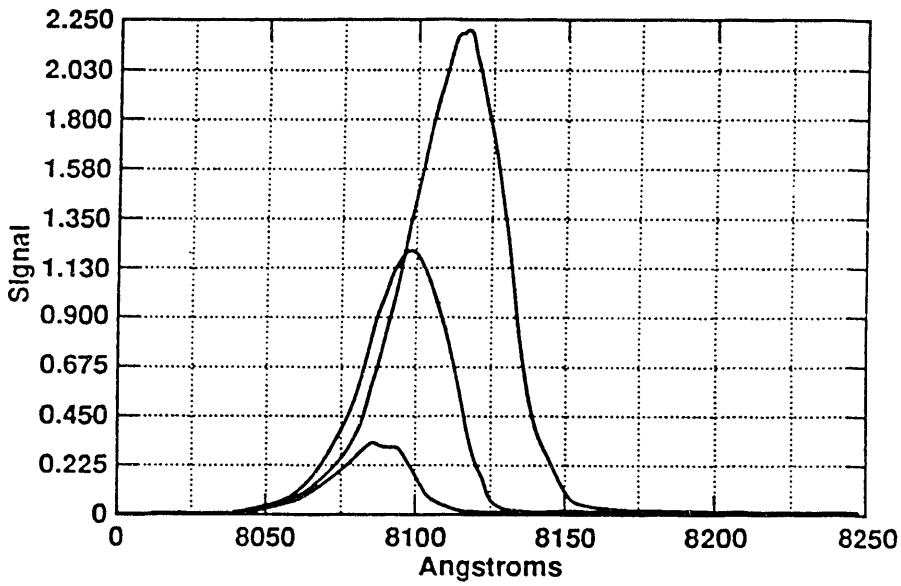

Figure 18

qt-u-j-16594-18

Fig 20

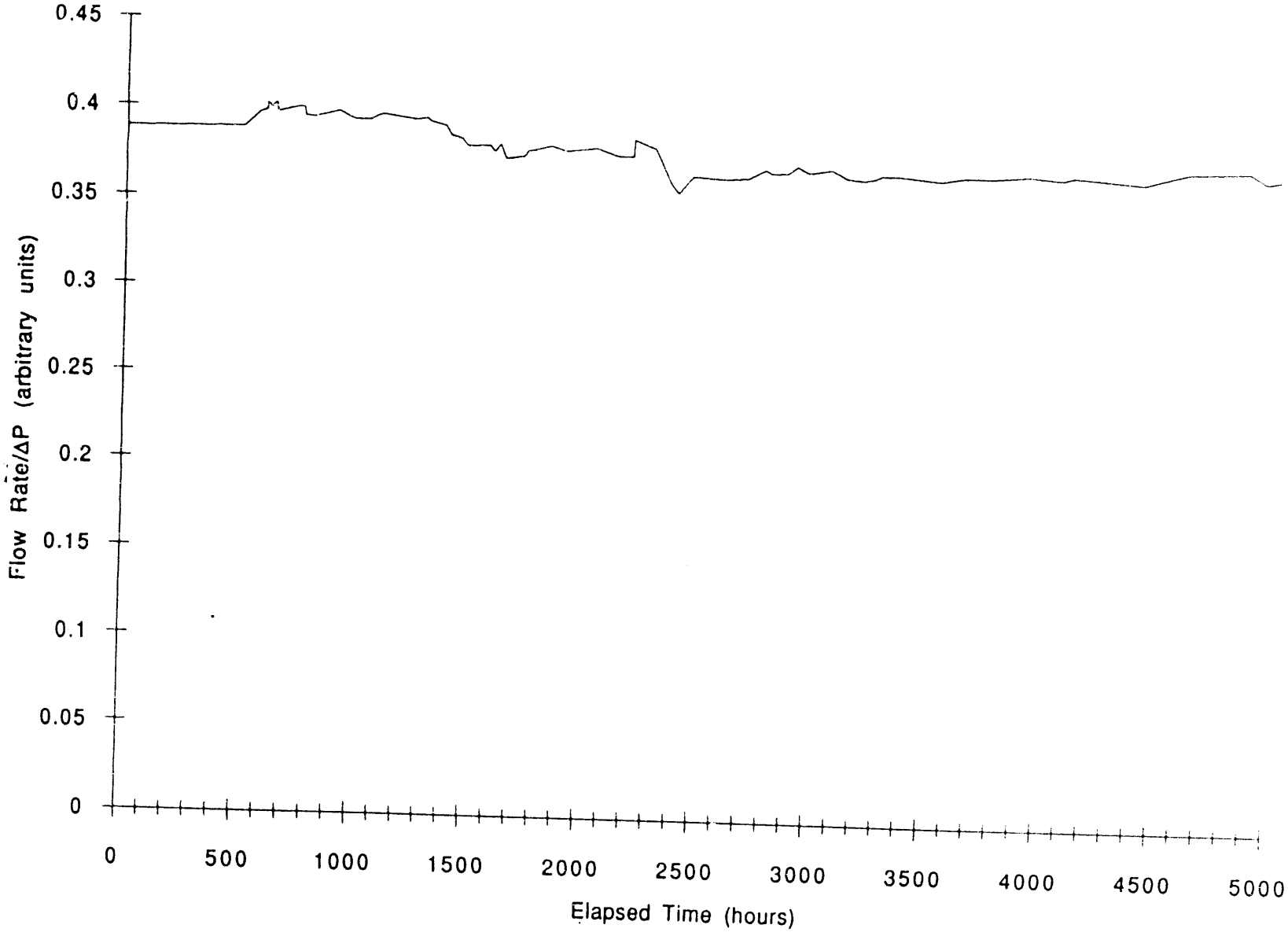
0.45
0.4
0.35
0.3
0.25
0.2
0.15
0.1
0.05
0
Flow Rate/ΔP (arbitrary units)
0
500
1000
1500
2000
2500
3000
3500
4000
4500
5000
Elapsed Time (hours)

END

DATE
FILMED
1/10/93